ECS Transactions, 2019, Vol.91, No.1, pp. 2387-2397, https://doi.org/10.1149/09101.2387ecst

Oxygen-Deficient $Nd_{0.8}Sr_{1.2}Ni_{0.8}M_{0.2}O_{4-\delta}$ (M = Ni, Co, Fe) Nickelates as Oxygen Electrode Materials for SOFC/SOEC

B.I. Arias-Serrano[a], E.S. Kravchenko[b], K. Zakharchuk[a], J. Grins[c], G. Svensson[c], V. Pankov[b], A.A. Yaremchenko[a]

[a] CICECO - Aveiro Institute of Materials, Department of Materials and Ceramic Engineering, University of Aveiro, 3810-193 Aveiro, Portugal
[b] Faculty of Chemistry, Belarusian State University, 220006 Minsk, Belarus
[c] Department of Materials and Environmental Chemistry, Stockholm University, 106 91 Stockholm, Sweden

Ruddlesden-Popper $Nd_{0.8}Sr_{1.2}Ni_{0.8}M_{0.2}O_{4-\delta}$ (M = Ni, Co, Fe) nickelates have been characterized as prospective oxygen electrode materials for solid electrolyte cells. XRD studies showed that these oxides retain tetragonal K_2NiF_4-type structure in air until at least 900°C. Average thermal expansion coefficients of $Nd_{0.8}Sr_{1.2}Ni_{0.8}M_{0.2}O_{4-\delta}$ calculated from the structural data are in the range 14.5-15.8 ppm/K. TGA studies revealed that these nickelates are oxygen-deficient in air at temperature above 700°C but tends to oxygen stoichiometry or minor excess on cooling. Incorporation of cobalt or iron into nickel sublattice of $Nd_{0.8}Sr_{1.2}NiO_{4-\delta}$ reduces oxygen deficiency and electrical conductivity. Electrochemical impedance spectroscopy studies of symmetrical cells showed that porous $Nd_{0.8}Sr_{1.2}Ni_{0.8}M_{0.2}O_{4-\delta}$ electrodes applied onto $Ce_{0.9}Gd_{0.1}O_{2-\delta}$ electrolyte exhibit quite similar performance, with lowest values of polarization resistance (0.8 $\Omega \cdot cm^2$ at 800°C) observed for M = Ni. The polarization resistance can be further decreased (down to 0.04 $\Omega \cdot cm^2$ at 800°C for M = Ni) by surface modification with PrO_x.

Introduction

Perovskite-related $Ln_2NiO_{4+\delta}$ (Ln = La, Pr, Nd) nickelates has layered K_2NiF_4-type structure and belong to the Ruddlesden-Popper (RP) series ($A_{n+1}B_nO_{3n+1}$, n = 1). This type of structure can be described as consisting of two-dimensional perovskite-type $LnNiO_3$ layers alternating with rock-salt-type LnO layers along the c axis and able to accommodate hyperstoichiometric oxygen in the form of interstitial oxygen ions located in the rock-salt LaO sheets (1,2). $Ln_2NiO_{4+\delta}$ nickelates and their derivatives have been demonstrated to combine redox stability (except undoped $Pr_2NiO_{4+\delta}$) with noticeable oxygen content changes yielding enhanced mixed ionic-electronic transport and electrocatalytic activity (2-4). These features attracted attention to these phases as promising materials for application as oxygen electrodes with good electrochemical performance for solid oxide fuel cells (SOFCs), solid oxide electrolysis cells (SOEC), protonic ceramic fuel cells (PCFCs), and reversible SOFC/SOEC systems (4-7).

To date, most efforts were focused on oxygen-hyperstoichiometric $Ln_2NiO_{4+\delta}$-based derivatives, whereas nickelates with oxygen-deficient lattice remain poorly explored. Undoped $Nd_2NiO_{4+\delta}$ has an orthorhombic K_2NiF_4-type structure (space group

Fmmm) with oxygen excess δ ~ 0.18-0.22 at room temperature (8,9). It undergoes a phase transition to the tetragonal structure (space group *I*4/*mmm*) on heating in air at 520–610°C accompanied by semiconductor-to-metal transition (9,10). Substitution of neodymium by strontium results in formation of a wide range of $Nd_{2-x}Sr_xNiO_{4\pm\delta}$ solid solutions, up to x = 1.60-1.66 (11,12). Increasing strontium content decreases the orthorhombic-to-tetragonal transition temperature (below room T for $x \geq 0.2$) and temperature of semiconductor-to-metal transition (below room T for $x > 0.7$), and is accompanied by a gradual transition from oxygen excess to stoichiometric oxygen content and then to oxygen deficiency (8,9,12,13). Since the acceptor-type substitution by strontium is partly compensated by the formation of electron-holes, this also has a positive effect on electrical conductivity. The highest conductivity in $Nd_{2-x}Sr_xNiO_{4\pm\delta}$ was reported for x = 1.2 composition (12). Increasing oxygen vacancy concentration with Sr content in Sr-rich composition is also expected to enhance the oxygen-ionic contribution to the total electrical transport, with a positive effect on electrocatalytic properties.

The present work aimed at the comparative high-temperature characterization of $Nd_{0.8}Sr_{1.2}Ni_{0.8}M_{0.2}O_{4-\delta}$ (M = Ni, Co, Fe) nickelates for the possible use as materials for oxygen electrodes of solid oxide cells. The emphasis was on the properties relevant for the oxygen electrode applications, including structural stability, oxygen nonstoichiometry and electrical conductivity, thermomechanical compatibility with solid electrolytes, and electrochemical performance of electrodes.

Experimental

Synthesis and Ceramic Processing

Powders of $Nd_{0.8}Sr_{1.2}Ni_{0.8}M_{0.2}O_{4-\delta}$ (M = Ni, Co, Fe) were synthesized by Pechini method using Nd_2O_3 (Alfa Aesar, 99.9% purity), $Sr(NO_3)_2$ (Sigma-Aldrich, 99% purity) and $Ni(NO_3)_2$*$6H_2O$ (Sigma-Aldrich, 98% purity) as starting reagents; the procedure is detailed in the previous work (12). The final steps included calcinations in flowing oxygen at 1150-1250°C for 20-30 h with several intermediate regrinding (T_{max} = 1200°C for M = Ni and 1250°C for M = Co and Fe). The powders were compacted uniaxially under ~40 MPa and sintered under oxygen atmosphere at 1250°C (M = Ni) or 1300°C (M = Co and Fe) for 5 h. Sintered ceramic samples were polished and cut into rectangular bars for dilatometric and electrical measurements.

Dense $Ce_{0.9}Gd_{0.1}O_{2-\delta}$ (CGO10) solid electrolyte pellets were prepared using commercial powder (CGO 90/10 UHSA, Anan Kasei Co., Japan). Disk-shaped samples were compacted uniaxially, sintered in air at 1600°C for 5 h, and then polished to thickness ~1.00 mm.

Materials Characterization

Room-temperature X-ray diffraction (XRD) patterns were recorded using Rigaku D/MAX-B (CuKα radiation) diffractometer. Variable-temperature XRD studies (25-900°C) were performed in air employing PANalytical X'Pert PRO MRD instrument (CuKα radiation) equipped with an Anton-Parr XRK900 reaction chamber. Rietveld refinement of the XRD data was done using FullProf software. Microstructural

characterization was performed by scanning electron microscopy (SEM, Hitachi SU-70 instrument) coupled with energy dispersive spectroscopy (EDS, Bruker Quantax 400 detector). Thermogravimetric analysis (TGA, Setaram SetSys 16/18 instrument) was carried out using powdered samples in flowing air with constant heating/cooling rate of 2°C/min. In order to determine the absolute oxygen content (4-δ) in oxides, the samples were reduced in a 10%H_2–90%N_2 flow at 950-1100°C to a mixture of Nd_2O_3, SrO and metallic M. Electrical conductivity (σ) in air was measured by the 4-probe DC method as function of temperature at 500-1000°C.

Electrode Fabrication and Electrochemical Studies

The electrode layers were prepared using as-synthesized $Nd_{0.8}Sr_{1.2}Ni_{0.8}M_{0.2}O_{4-\delta}$ powders. For the preparation of electrode inks, each nickelate powder was mixed with a solvent (α-terpineol, 30:70 vol.% ratio) with additions of a binder (ethyl cellulose, 5 wt.%) and a dispersant (stearic acid, 3 wt%) and ball-milled for several hours. Porous electrode layers (diameter 5 mm) were painted on both side of electrolyte pellets in symmetrical configuration and sintered at 1050°C for 2 h in air. Surface density of porous electrode layers was 8-11 mg/cm^2. The surface modification of electrode layers was performed by infiltration of a saturated ethanol solution of praseodymium nitrate with subsequent calcination at 800°C for 2 h. The polarization resistance of electrode layers in contact with CGO10 solid electrolyte was determined in air at 600-800°C (cooling regime with equilibration at each temperature) employing electrochemical impedance spectroscopy (EIS, Autolab PGSTAT302 instrument with built-in FRA module, frequency range 10 mHz - 1 MHz, amplitude 50 mV). Pt gauze with Pt wires was used for current collectors.

Results and Discussion

XRD analysis confirmed the formation of solid solutions with the K_2NiF_4-type tetragonal structure (space group *I*4/*mmm*) for all prepared compositions. Both synthesized powders and sintered ceramics were phase-pure in the case of M = Ni and Fe. Negligible peaks of NiO impurity were visible in XRD patterns at the background level for Co-containing samples. The partial substitution of nickel by cobalt or iron has a comparatively minor effect on the tetragonal lattice parameter *a*, but results in an elongation of the crystal lattice along the *c* axis in a row Ni < Co < Fe (Table I).

TABLE I. Room-temperature lattice parameters and density of prepared $Nd_{0.8}Sr_{1.2}Ni_{0.8}M_{0.2}O_{4-\delta}$ ceramics.

M	Lattice parameters		Density, g/cm^3	Relative density, %*
	a, nm	*c*, nm		
Ni	3.8037(1)	12.2587(1)	5.40	84
Co	3.7992(1)	12.2961(2)	4.25	66
Fe	3.8058(1)	12.3446(3)	4.15	65

* Theoretical density was calculated neglecting oxygen nonstoichiometry (δ = 0).

High-temperature XRD studies at 25-900°C confirmed that all prepared materials retain tetragonal K_2NiF_4-type structure (space group *I*4/*mmm*) in the studied temperature range in air. Examples of the XRD patterns for one of the compositions are given in Figure 1.

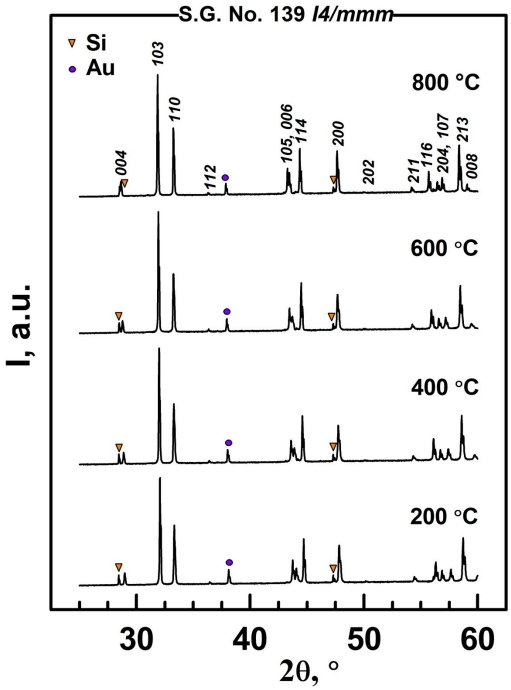

Figure 1. Examples of XRD patterns of $Nd_{0.8}Sr_{1.2}Ni_{0.8}Co_{0.2}O_{4-\delta}$ collected on heating in air. Reflections are indexed in the *I*4/*mmm* space group. Triangles and circles mark the peaks of Si standard and Au substrate, respectively.

Calculations of the lattice parameters revealed strongly anisotropic expansion of the tetragonal lattice on heating: faster elongation along *c* axis compared to expansion in *a*-*b* plane, in agreement with the previous results on Sr-rich $Ln_{2-x}Sr_xNiO_{4\pm\delta}$ (Ln = La, Nd; x = 1.0-1.6) series (12,14). In the XRD patterns, this is reflected by a greater shift of the (00*l*) reflections to lower angles with increasing temperature if compared to other peaks (Figure 1).

Sintering at 1250-1300°C produced porous ceramic samples with relative density ~84% for M = Ni and ~65% for M = Co and Fe (Table I). The attempts to increase the sintering temperature to 1350-1400°C were not successful: this promoted the grain growth and crack formation and yielded fragile samples that easily crashed into powder on touch. Such behavior originates from the strongly anisotropic expansion of the tetragonal lattice of Sr-rich nickelates and associated microcracking effects, as discussed in the previous reports (12,14). Note that these effects should not be critical in the case of porous electrode layers with a smaller particle size and higher porosity if compared to sintered ceramic compacts.

Microcracking effects are also known to result in a specific shape of dilatometric curves with a significant hysteresis on temperature cycling due to the contributions of "healing" (a closure) of microcracks on heating and their reopening on cooling (12,14,15). This makes impossible to determine the thermal expansion coefficients (TECs) of nickelate ceramics from direct dilatometric experiments. Therefore, in this work, the average linear TEC values were calculated from the high-temperature XRD results. The calculated TECs (Table II) are slightly higher but generally comparable to those of $Ln_2NiO_{4+\delta}$-based nickelate ceramics and other RP phases (4,16). Substitution of nickel by cobalt has a rather minor effect, while the incorporation of iron into the nickel sublattice

results in a favorably smaller thermal expansion coefficient (Table II). TECs of all compositions still exceeds that of CGO10 solid electrolyte; the difference is however relatively small. This is expected to ensure the thermomechanical compatibility of nickelate electrode layers and ceria-based electrolyte ceramics under oxidizing conditions.

TABLE II. Average thermal expansion coefficients of $Nd_{0.8}Sr_{1.2}Ni_{0.8}M_{0.2}O_{4-\delta}$ nickelates in air*.

M	T, °C	TEC, ppm/K
Ni	25-900	15.6 ± 0.2
Co	25-900	15.8 ± 0.4
Fe	25-900	14.5 ± 0.4
CGO10 (17)	25-1100	12.4

* Calculated from the variable-temperature XRD data.

Thermogravimetric studies demonstrated that all $Nd_{0.8}Sr_{1.2}Ni_{0.8}M_{0.2}O_{4-\delta}$ lose weight on heating in air. This originates from the reversible reduction of transition metal cations on heating and accompanied oxygen release from the crystal lattice:

$$2M^{(n+1)+} + O_i^{2-} \leftrightarrow 2M^{n+} + 0.5O_2 \quad [1]$$

or

$$2M^{(n+1)+} + O_O^{2-} \leftrightarrow 2M^{n+} + V_O + 0.5O_2 \quad [2]$$

where O_i^{2-}, O_O^{2-} and V_O are interstitial oxygen ion, oxygen ion in a regular lattice site and oxygen vacancy, respectively.

Analysis of the thermogravimetric data indicated that all prepared $Nd_{0.8}Sr_{1.2}Ni_{0.8}M_{0.2}O_{4-\delta}$ nickelates are oxygen-deficient (*i.e.* oxygen vacancy is dominating oxygen defect) in air at temperatures above 700°C (Figure 2), but tend to stoichiometric oxygen content ($\delta = 0$) or even slight oxygen excess at lower temperatures. Substitution of nickel by iron or cobalt decreases the oxygen vacancy concentration in the high-temperature range, with a stronger effect in the case of cobalt incorporation into the nickel sublattice. Earlier, a similar increase in oxygen content due to substitution by cobalt or iron into nickel sublattice was reported for related oxygen-hyperstoichiometric $La_2Ni_{0.9}M_{0.1}O_{4+\delta}$ (18,19).

Simple estimations (assuming that all oxygen ions in the lattice are doubly charged) indicate that average oxidation state of nickel cations in $Nd_{0.8}Sr_{1.2}Ni_{0.8}M_{0.2}O_{4-\delta}$ in air is slightly below 3+ at 900-950°C and is above 3+ at temperatures ≤ 850°C. In the case of Co- and Fe-substituted compositions, the average oxidation state of B-site cations is above 3+ in the entire studied temperature range, although one may reasonably expect that average charge of substituting cations in these oxides exceeds that of the host Ni ions. The data on electrical conductivity of $Nd_{0.8}Sr_{1.2}Ni_{0.8}M_{0.2}O_{4-\delta}$ in air are given in Figure 3. One should note that the measurements were done using highly porous ceramic samples. On the one hand, this should yield underestimated conductivity of the oxide materials, but, on the other hand, provides the values of electrical conductivity of porous bodies with a porosity comparable to that of porous electrode layers.

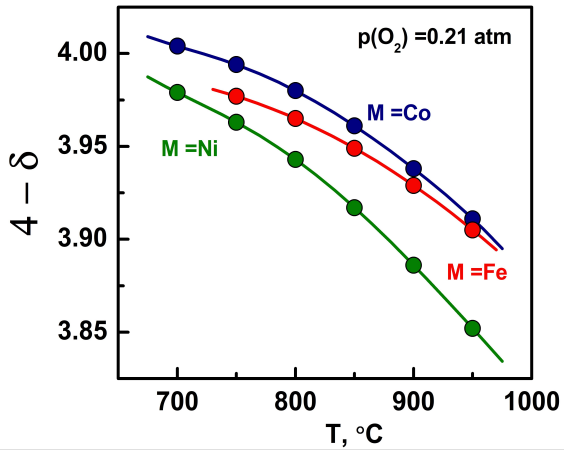

Figure 2. Equilibrium values of oxygen nonstoichiometry in $Nd_{0.8}Sr_{1.2}Ni_{0.8}M_{0.2}O_{4-\delta}$ nickelates in air calculated from the results of thermogravimetric studies.

All studied materials exhibit metallic-like behavior of electrical conductivity which decreases on heating. Metallic-like conduction in $Ln_{2-x}Sr_xNiO_{4\pm\delta}$ is believed to occur via free electron-holes in the $\sigma_{x^2-y^2}$ band formed by delocalized $d_{x^2-y^2}$ Ni orbitals (9,13). Heating above 700°C promotes oxygen losses from the lattice (Figure 2) accompanied by a decrease in the concentration of *p*-type electronic charge carriers and their mobility (due to increasing concentration of broken Ni-O chains in basal plane). Assuming $Nd_2^{3+}Ni^{2+}O_4^{2-}$ as a host lattice, the electroneutrality condition for $Nd_{0.8}Sr_{1.2}Ni_{0.8}M_{0.2}O_{4-\delta}$ nickelates may be expressed by (using Kröger-Vink notation):

$$[Sr'_{Nd}] + 2[O''_i] = [M^{\bullet}_{Ni}] + 2[M^{\bullet\bullet}_{Ni}] + 2[V^{\bullet\bullet}_O] \quad [3]$$

or

$$p = 1.2 - 2\delta \quad [4]$$

where *p* is the concentration of electron-holes (per formula unit) formally residing on B-site cations, *i.e.* $M^{\bullet}_{Ni} \equiv M^{3+}$ and $M^{\bullet\bullet}_{Ni} \equiv M^{4+}$, and δ indicates oxygen deficiency, *i.e.* $\delta = [V^{\bullet\bullet}_O] - [O''_i]$. Thus, increasing oxygen deficiency of heating above ~700°C facilitates the decline of electrical conductivity and results in a change of slope of *log σ – 1/T* curves (Figure 3).

The partial substitution of nickel by cobalt or iron has a negative effect on the conductivity of $Nd_{0.8}Sr_{1.2}Ni_{0.8}M_{0.2}O_{4-\delta}$ ceramics. At 800°C, the measured conductivity values drop from ~400 S/cm for M = Ni to 150 S/cm for M = Co and to 65 S/cm for M = Fe. Apparently, incorporation of cobalt or iron into nickel sublattice promotes the localization of electron-holes, thus decreasing their mobility, or trapping of charge carriers on substituting cations (18,19). Contrary to Ni-based counterparts (12,14), RP-type $(Ln,Sr)CoO_{4\pm\delta}$ (20,21) and $(Ln,Sr)FeO_{4\pm\delta}$ (22) phases exhibit temperature-activated electrical transport occurring via small polaron hopping mechanism. Still, the electrical conductivity of $Nd_{0.8}Sr_{1.2}Ni_{0.8}M_{0.2}O_{4-\delta}$ ceramics is sufficiently high, even for Fe-substituted nickelate, to not be a performance-limiting factor, especially given that the values were obtained for quite porous samples.

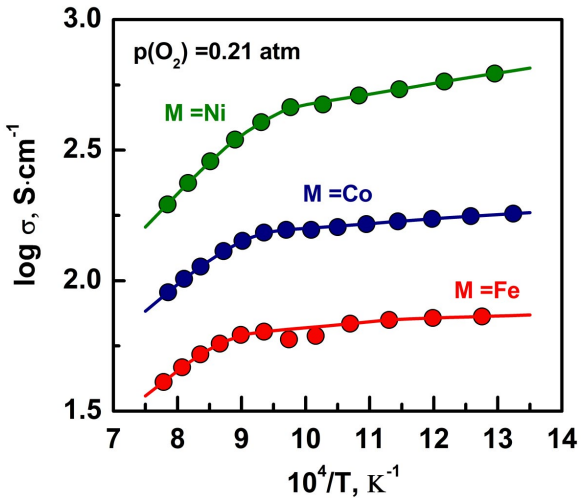

Figure 3. Temperature dependence of electrical conductivity of $Nd_{0.8}Sr_{1.2}Ni_{0.8}M_{0.2}O_{4-\delta}$ ceramics in air.

Porous electrode layers for electrochemical studies were prepared using as-synthesized powder (highest calcination temperature was 1200°C for M = Ni and 1250°C for M = Co and Fe) and sintered at 1050°C for 2 h. The electrode sintering conditions were selected based on previous results for similar electrode materials (14) to ensure sufficient mechanical stability while minimizing the reactivity between electrode and electrolyte materials. Figure 4(A-C) compares the microstructure of prepared electrodes. $Nd_{0.8}Sr_{1.2}NiO_{4-\delta}$ electrodes had the finest microstructure with particle of 0.5-2.0 μm in diameter partly aggregated in large agglomerates (Figure 4C). Cobalt- and iron-containing compositions required higher calcination temperature to obtain phase-pure nickelates, and this promoted grain growth, especially in the case of $Nd_{0.8}Sr_{1.2}Ni_{0.8}Co_{0.2}O_{4-\delta}$ powder yielding electrode layers with particle size in the range from ~0.5 μm up to 5 μm (Figure 4A).

Typical impedance spectra of $Nd_{0.8}Sr_{1.2}Ni_{0.8}M_{0.2}O_{4-\delta}$ in contact with CGO10 solid electrolyte collected in air under zero-current conditions are shown in Figure 5A. The shape of spectra suggests at least two contributions to the electrode process; the spectra were fitted using a simple equivalent circuit $L\text{-}R_{Ohm}\text{-}(R_{HF}||CPE_{HF})\text{-}(R_{LF}||CPE_{LF})$ where $(R_{HF}+R_{LF})$ constitutes the electrode polarization resistance R_p.

All three compositions demonstrated rather similar electrochemical activity (Figure 5A, Figure 6 and Table III). The polarization resistance was lowest in the case of M = Ni, 0.8 Ohm×cm^2 at 800°C, and increased slightly in a row Ni < Fe < Co, in agreement with the variation of the particle size (and, therefore, active surface area) and oxygen vacancy concentration. Earlier, the polarization resistance of related $La_{2-x}Sr_xNiO_{4-\delta}$ (x = 0.5-0.8) electrodes was observed to decrease with increasing oxygen deficiency δ (presumably, due to increasing ionic contribution to the total conductivity of nickelates) (14). All materials exhibit also the same activation energy of the electrode process, within the limits of experimental uncertainty (Table III). Furthermore, the electrode performance of $Nd_{0.8}Sr_{1.2}Ni_{0.8}M_{0.2}O_{4-\delta}$ is better compared to $La_{0.8}Sr_{1.2}NiO_{4-\delta}$ counterpart applied onto CGO10 and sintered under similar conditions (14), but worse if compared to optimized $La_2NiO_{4+\delta}$ based electrodes reported in literature (*e.g.* Refs.(5,6)).

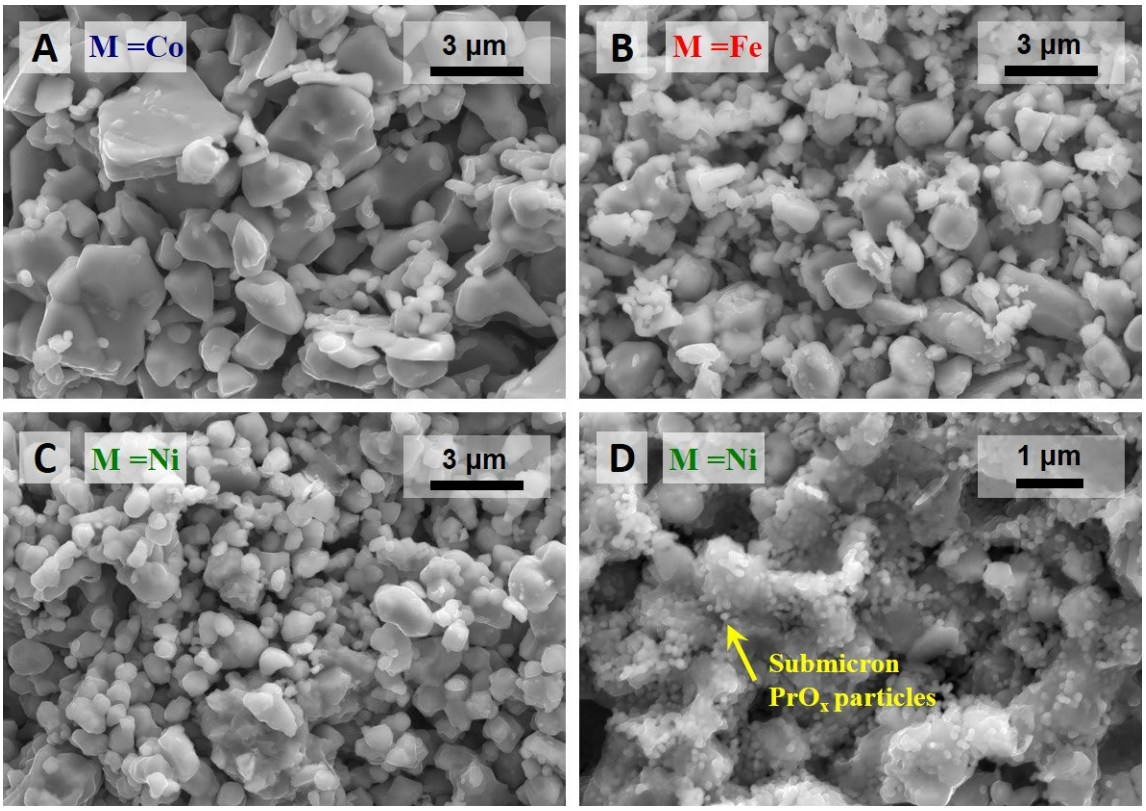

Figure 4. Microstructure of porous electrode layers: (A-C) $Nd_{0.8}Sr_{1.2}Ni_{0.8}M_{0.2}O_{4-\delta}$ electrodes; (D) $Nd_{0.8}Sr_{1.2}NiO_{4-\delta}$ electrode modified with praseodymia.

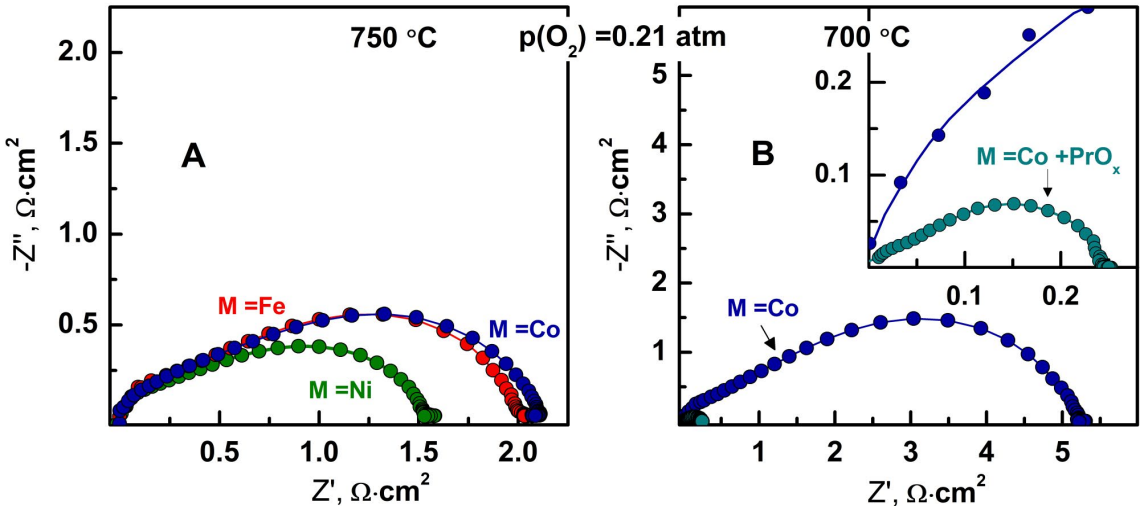

Figure 5. Impedance spectra under zero-current conditions in air: (A) $Nd_{0.8}Sr_{1.2}Ni_{0.8}M_{0.2}O_{4-\delta}$ electrodes at 750°C; (B) bare and praseodymia-modified $Nd_{0.8}Sr_{1.2}Ni_{0.8}Co_{0.2}O_{4-\delta}$ electrodes at 700°C. The spectra were corrected for ohmic resistance.

The electrochemical performance of $Nd_{0.8}Sr_{1.2}Ni_{0.8}M_{0.2}O_{4-\delta}$ electrodes was improved by surface modification via infiltration of praseodymia. Under oxidizing conditions, praseodymium (III,IV) oxide is a mixed ionic-electronic conductor with high oxygen diffusion and surface exchange coefficients and is considered as an effective

electrocatalyst for the oxygen reduction reaction (23,24). Infiltration of praseodymium nitrate solution into $Nd_{0.8}Sr_{1.2}Ni_{0.8}M_{0.2}O_{4-\delta}$ electrodes with subsequent thermal decomposition of nitrate produced a layer of submicron PrO_x particles (100-200 nm) covering the surface of nickelate particles (Figure 4D).

The modification of electrode layer with praseodymia resulted in substantial drop of polarization resistance, by a factor of 15-20 at 800°C (Figs.5B and 6). In the case of M = Ni, the polarization resistance decreased from 0.79 Ohm×cm^2 for the bare electrode to 0.04 Ohm×cm^2 for the modified electrode (Table III). This was accompanied by a decrease in the activation energy of electrode process (Table III) leading to even better improvement at lower temperatures. As for the unmodified electrodes, the best electrochemical performance after infiltration of PrO_x was observed for $Nd_{0.8}Sr_{1.2}NiO_{4-\delta}$, while Co- and Fe-containing electrode materials showed very similar activity (Figure 6 and Table III). Once again, this can be attributed, most likely, to the microstructural differences as a main factor, with the PrO_x fraction being another important factor. A smaller particle size in the case of M = Ni apparently provides higher active surface area of nickelate-supported PrO_x electrocatalyst. Thus, the future work should include the optimization of the electrode microstructure (via optimization of synthesis and sintering conditions) and praseodymium oxide fraction.

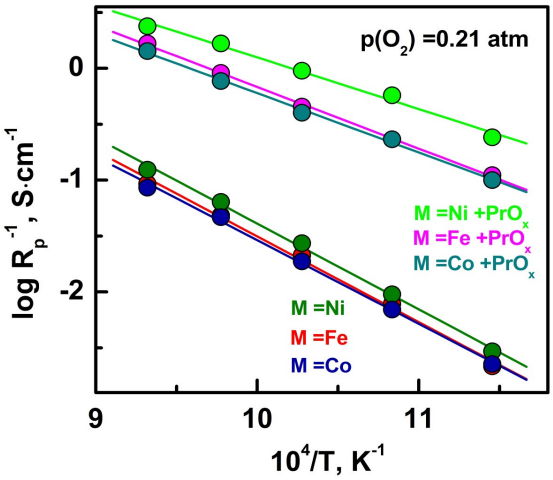

Figure 6. Temperature dependence of polarization resistance R_p of $Nd_{0.8}Sr_{1.2}Ni_{0.8}M_{0.2}O_{4-\delta}$ electrodes in contact with CGO10 solid electrolyte under zero-current conditions in air.

TABLE III. Polarization resistance of $Nd_{0.8}Sr_{1.2}Ni_{0.8}M_{0.2}O_{4-\delta}$ electrodes in contact with CGO10 electrolyte.

Electrode	PrO_x, wt.%	R_p, Ohm×cm^2			E_A, kJ/mol
		800°C	700°C	600°C	(600-800°C)
M = Ni		0.79	3.6	33.4	155 ± 4
M = Co		1.15	5.2	43.3	150 ± 3
M = Fe		1.04	4.6	45.4	155 ± 6
M = Ni + PrO_x	23	0.04	0.10	0.41	96 ± 5
M = Co + PrO_x	21	0.07	0.25	0.98	110 ± 3
M = Fe + PrO_x	17	0.06	0.22	0.88	114 ± 2

Note: The activation energy E_A is calculated using Arrhenius equation $1/R_p = (A_0/T)\exp(-E_A/(RT))$.

Conclusions

$Nd_{0.8}Sr_{1.2}Ni_{0.8}M_{0.2}O_{4-\delta}$ nickelates retain tetragonal K_2NiF_4-type structure in air from room temperature up to at least 900°C. Thermogravimetric studies demonstrated that these oxides are oxygen-deficient in air at temperatures above 700°C but tend to stoichiometric oxygen content or even slight oxygen excess at lower temperatures. Incorporation of cobalt or iron into nickel sublattice of $Nd_{0.8}Sr_{1.2}NiO_{4-\delta}$ reduces oxygen nonstoichiometry, total electrical conductivity and, to some extent, thermal expansion (in the case of Fe-substitution). The average thermal expansion coefficients of $Nd_{0.8}Sr_{1.2}Ni_{0.8}M_{0.2}O_{4-\delta}$ are in the range 14.5-15.8 ppm/K at 25-900°C being close to that of doped ceria. Porous $Nd_{0.8}Sr_{1.2}Ni_{0.8}M_{0.2}O_{4-\delta}$ electrode layers sintered at 1050°C demonstrate quite similar performance in contact with CGO10 solid electrolyte. The lowest electrode polarization resistance (R_p = 0.8 Ohm×cm^2 at 800°C) under zero-current conditions was found for M = Ni electrodes, in correlation with the microstructural characteristics and oxygen vacancy concentration. The electrochemical activity of $Nd_{0.8}Sr_{1.2}Ni_{0.8}M_{0.2}O_{4-\delta}$ electrodes can be substantially improved by surface modification with PrO_x, resulting in more than one order of magnitude drop of polarization resistance values (down to 0.04 Ohm×cm^2 at 800°C for M = Ni).

Acknowledgements

This work was done within the scope of project CARBOSTEAM (POCI-01-0145-FEDER-032295) and project CICECO - Aveiro Institute of Materials (FCT ref. UID/CTM/50011/2019), financed by national funds through the FCT/MCTES and when appropriate co-financed by FEDER under the PT2020 Partnership Agreement.

References

1. M. Greenblatt, *Curr. Opin. Colloid Solid State Mater. Sci.*, **2**, 174 (1997).
2. D. Lee and H.N. Lee, *Materials*, **10**, 368 (2017).
3. A. Das, E. Xhafa and E. Nikolla, *Catal. Today*, **277**, 214 (2016).
4. H. Zhao, Q. Li and L.P. Sun, *Sci. China Chem.*, **54**, 898 (2011).
5. T. Ogier, F. Mauvy, J. M. Bassat, J. Laurencin, J. Mougin and J. C. Grenier, *Int. J. Hydrogen Energy*, **40**, 15885 (2015).
6. B. Philippeau, F. Mauvy, C. Mazataud, S. Fourcade and J. C. Grenier, *Solid State Ionics*, **249-250**, 17 (2013).
7. A. Tarutin, J. Lyagaeva, A. Farlenkov, S. Plaksin, G. Vdovin, A. Demin and D. Medvedev, *Materials*, **12**, 18 (2019).
8. M.P. Sridhar Kumar, S.M. Doyle and D. McK Paul, *J. Less-Common Met.*, **164-165**, 920 (1990).
9. Y. Takeda, M. Nishijima, N. Imanishi, R. Kanno, O. Yamamoto and M. Takano, *J. Solid State Chem.*, **96**, 72 (1992).
10. E. Boehm, J.M. Bassat, P. Dordor, F. Mauvy, J.C. Grenier and P. Stevens, *Solid State Ionics*, **176**, 2717 (2005).
11. M. James and J. P. Attfield, *J. Mater. Chem.*, **6**, 57 (1996).
12. E. Kravchenko, D. Khalyavin, K. Zakharchuk, J. Grins, G. Svensson, V. Pankov and A. Yaremchenko, *J. Mater. Chem. A*, **3**, 23852 (2015).

13. B. W. Arbuckle, K. V. Ramanujachary, Z. Zhang and M. Greenblatt, *J. Solid State Chem.*, **88**, 278 (1990).
14. E. Kravchenko, K. Zakharchuk, A. Viskup, J. Grins, G. Svensson, V. Pankov and A. Yaremchenko, *ChemSusChem*, **10**, 600 (2017).
15. H. A. J. Thomas and R. Stevens, *Br. Ceram. Trans. J.*, **88**, 144 (1989).
16. M. Al Daroukha, V.V. Vashooka, H. Ullmanna, F. Tietzb and I. Arual Raj, *Solid State Ionics*, **158**, 141 (2003).
17. A.A. Yaremchenko, S.M. Mikhalev, E.S. Kravchenko and J.R. Frade, *J. Eur. Ceram. Soc.*, **34**, 703 (2014).
18. V.V. Kharton, E.V. Tsipis, E.N. Naumovich, A. Thursfield, M.V. Patrakeev, V.A. Kolotygin, J.C. Waerenborgh and I.S. Metcalfe, *J. Solid State Chem.*, **181**, 1425 (2008).
19. E.N. Naumovich, M.V. Patrakeev, V.V. Kharton, A.A. Yaremchenko, D.I. Logvinovich and F.M.B. Marques, *Solid State Sci.*, **7**, 1353 (2005).
20. F. Riza and Ch. Ftikos, *J. Eur. Ceram. Soc.*, **27**, 571 (2007).
21. C. Tealdi, C. Ferrara, L. Malavasi, P. Mustarelli, C. Ritter, G. Chiodelli and Y.A. Diaz-Fernandez, *Phys. Rev. B*, **82**, 174118 (2010).
22. J. Zhou, Y. Chen, G. Chen, K. Wu and Y. Cheng, *J. Alloy Compd.*, **647**, 778 (2015).
23. C. Nicollet, A. Flura, V. Vibhu, A. Rougier, J.M. Bassat and J.C. Grenier, *Int. J. Hydrogen Energy*, **41**, 15538 (2016).
24. H. Taguchi, R. Chiba, T. Komatsu, H. Orui, K. Watanabe and K. Hayashi, *J. Power Sources*, **241**, 768 (2013).